# Far-infrared and dc magnetotransport of CaMnO_{3}-CaRuO_{3} superlattices

P. Yordanov, A. V. Boris, J. W. Freeland, J. J. Kavich, J. Chakhalian, H. N. Lee, and B. Keimer

Phys. Rev. B **84**, 045108 — Published 7 July 2011

DOI: 10.1103/PhysRevB.84.045108

# Far-infrared and *dc*-Magnetotransport of $CaMnO_3$ – $CaRuO_3$ Superlattices

P. Yordanov[1], A.V. Boris[1], J.W. Freeland[2], J.J. Kavich[2], J. Chakhalian[3], H.N. Lee[4] and B. Keimer[1]
[1]*Max-Planck-Institut für Festkörperforschung, D-70569 Stuttgart, Germany*
[2]*Advanced Photon Source, Argonne National Laboratory, Argonne, IL 60439, USA*
[3]*Department of Physics, University of Arkansas, Fayetteville, AR 72701, USA and*
[4]*Materials Science and Technology Division, Oak Ridge National Laboratory, Oak Ridge, TN 37831, USA*

We report temperature and magnetic field dependent measurements of the *dc* resistivity and the far-infrared reflectivity (photon energies $\hbar\omega = 50 - 700$ cm$^{-1}$) of superlattices comprising 10 consecutive unit cells of the antiferromagnetic insulator $CaMnO_3$, and 4 – 10 unit cells of the correlated paramagnetic metal $CaRuO_3$. Below the Néel temperature of $CaMnO_3$, the *dc* resistivity exhibits a logarithmic divergence upon cooling, which is associated with a large negative, isotropic magnetoresistance. The $\omega \rightarrow 0$ extrapolation of the resistivity extracted from the FIR reflectivity, on the other hand, shows a much weaker temperature and field dependence. We attribute this behavior to scattering of itinerant charge carriers in $CaRuO_3$ from sparse, spatially isolated magnetic defects at the $CaMnO_3$-$CaRuO_3$ interfaces. This field-tunable "transport bottleneck" effect may prove useful for functional metal-oxide devices.

PACS numbers: 73.21.Cd, 75.70.Cn, 73.20.-r

## I. INTRODUCTION

Magnetoresistance phenomena in multilayer structures have attracted widespread attention following the discovery of the "giant magnetoresistance" (GMR) effect in heterostructures comprising metals that exhibit negligible magnetoresistance (MR) in the bulk. Recently, related phenomena have also been discovered in heterostructures composed of transition metal oxides, including superlattices of the antiferromagnetic insulators $LaMnO_3$ and $SrMnO_3$ that replicate the "colossal magnetoresistance" (CMR) effect in the corresponding solid solution[1–3], bilayer structures of the two band insulators $LaAlO_3$ and $SrTiO_3$ with a metallic interface subject to Rashba spin-orbit interactions[4,5], and superlattices of the correlated metal $CaRuO_3$ and the antiferromagnetic insulator $CaMnO_3$.[6,7] Like the original GMR effect, the sign and magnitude of the MR in oxide heterostructures is expected to be influenced both by the electronic structure of the bulk constituents and by interfacial defects, but it is difficult to discriminate between both factors based on *dc*-MR measurements alone. Spectroscopic methods, on the other hand, can supply general information about interfacial defects, but rarely yield specific insights into their contribution to the magnetotransport properties. Consequently, the microscopic origin of MR phenomena in oxide heterostructures remains largely unexplored.

Here we report the observation of a large negative *dc*-magnetoresistance effect in superlattices composed of $CaRuO_3$ (Refs. 8–11) and $CaMnO_3$ (Refs. 12–15) and show that a comparison between far-infrared and *dc*-MR measurements can yield insights into the origin of this behavior. Interest in this system was sparked by the discovery of interface ferromagnetism for temperatures below the Néel temperature of the $CaMnO_3$ layers.[6,7] This effect was attributed to a transfer of charge carriers from $CaRuO_3$ across the interface into an atomically thin layer of $CaMnO_3$, where they induce spin canting via the double-exchange interaction (Fig. 1). This scenario was supported by density functional calculations[16] and by a detailed spectroscopic study[17]. However, the magnetization profile determined by reflectometry with circularly polarized x-rays[17] revealed that the ferromagnetic magnetization penetrates more deeply into the $CaMnO_3$ layers than predicted by the *ab-initio* theory, possibly as a consequence of the formation of magnetic polarons that have also been invoked to explain experiments on bulk doped $CaMnO_3$.[12–15,18]

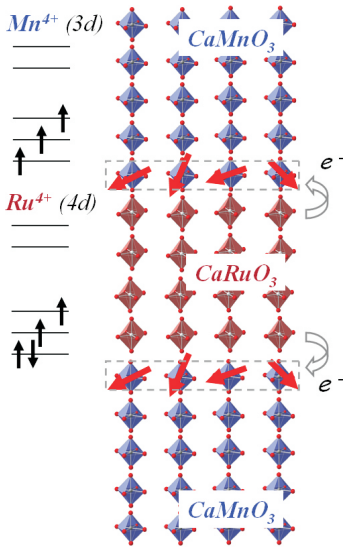


FIG. 1: Schematic picture of a $CaMnO_3$ - $CaRuO_3$ superlattice. The sketch on the left displays the nominal electron configuration of the constituents: $CaMnO_3$ in the high-spin state with $S = 3/2$, and $CaRuO_3$ in low-spin state with $S = 1$. Leakage of itinerant electrons from $CaRuO_3$ into $CaMnO_3$ induces canting of antiferromagnetically correlated Mn spins close to the interfaces.

In view of the converging experimental and theoretical descriptions, $CaRuO_3$-$CaMnO_3$ superlattices are suitable as a model system for spin-dependent transport phenomena in artificially structured oxides. Takahashi *et al.*[6] already noted a negative *dc*-MR of about 5% in a magnetic field of 5 T. In contrast to the CMR effect in bulk oxide ferromagnets, this effect persists far below the magnetic ordering temperature. This

was attributed to scattering of charge carriers from canted Mn spins at the interface, whose presence was confirmed in subsequent spectroscopic experiments.[17] It has remained unclear, however, to what extent this effect is influenced by interfacial defects that may act as "bottlenecks" for the $dc$ charge transport. In order to elucidate this issue, we have carried out accurate far-infrared (FIR) reflectance experiments as a function of magnetic field. Since the FIR conductivity extracted from these measurements does not require a continuous current path through the entire superlattice, it is much less affected by extended defects such as dislocations and stacking faults, which are nearly unavoidable in multilayer systems. A comparison between FIR and $dc$ transport data on $CaMnO_3$-$CaRuO_3$ superlattices indeed indicates a substantial enhancement of the $dc$-MR by spin textures nucleated at extended defects.

The paper is organized as follows. Details of the superlattice samples and the experimental setup are described in Section II. In Section III.A we report the $dc$ transport experiments on the superlattices and reference measurements on $CaMnO_3$ and $CaRuO_3$ films. Section III.B contains a description of the FIR experiments, and Section IV provides a summary of the conclusions.

## II. EXPERIMENTAL DETAILS

Superlattices with 6 bilayers comprising 10 consecutive unit cells (u.c.) of $CaMnO_3$ and $N = 4$ and 10 u.c. of $CaRuO_3$, respectively, were prepared using pulsed-laser deposition on $LaAlO_3$ (001) substrates. Details of the growth conditions are given in Ref. 17. The structural and electronic properties of the samples investigated here have been characterized extensively by a combination of experimental probes including magnetometry, spectral ellipsometry, x-ray reflectometry, x-ray absorption spectroscopy, x-ray magnetic circular dichroism, and x-ray resonant magnetic scattering.[17] Briefly, the films are well ordered and fully epitaxial, so that dislocations induced by twin boundaries on the substrate surface[19] must be sparse and localized at the atomic scale. Both superlattices exhibit ferromagnetic signals due to canted Mn spins below the Néel temperature $T_N = 125$ K , whereas no spin polarization was observed on Ru.

The FIR reflectivity measurements were conducted using a custom-built near-normal incidence infrared spectrometer. The apparatus consists of a Fourier Transform interferometer (Bruker IFS 66v/S) with spectral resolution of 0.5 $cm^{-1}$ attached to an 8 T superconducting split-coil magnet system (Oxford Spectromag SM 4000). The configuration to cover the FIR range includes a Hg-arc lamp, a multilayer Bruker T222 beamsplitter, and a IRLabs Si bolometer kept at a temperature of 1.8 K. The sample was placed in the variable temperature insert of the Spectromag system with accessible range 1.6 - 300 K. The reflectivity spectra were referenced against a gold mirror.

The $dc$-transport measurements were performed in a Physical Properties Measurement System (Quantum Design) equipped with an 8 T superconducting magnet. The contacts were made by silver paint in a linear four-point geometry. The contact size was $\sim 0.5$ mm with a spacing of 1 mm, so that the transport measurements average over any microstructure induced by twin boundaries on the $LaAlO_3$ substrate (with typical spacings 1-100 $\mu$m). The measurements were made with currents ranging from 10-100 nA. The resistivity of the films and superlattices was calculated according to $\rho = R_S \times d$, where $R_S$ is the measured sheet resistance and $d$ is the sample thickness determined by monitoring the intensity oscillation of the reflection high-energy diffraction pattern during growth, and confirmed by x-ray reflectometry.

## III. RESULTS AND DISCUSSION

### A. $dc$ Transport

Before reporting the results of the $dc$ transport measurements on the superlattice samples, we first describe reference measurements on $CaRuO_3$ and $CaMnO_3$ films grown under the same conditions. The $CaRuO_3$ film (Fig. 2) exhibits metallic resistivity with a non-Fermi-liquid temperature dependence best described by a sub-linear form in its high-temperature range above 60 K, $\rho(T) \propto T^{\alpha}$ with $\alpha = 0.74$, in qualitative agreement with prior work that had yielded power-law exponents $\alpha = 1/2$ and $3/2$ for the high- and low-temperature ranges, respectively.[8–11] This has been ascribed to the influence of spin fluctuations in proximity to a ferromagnetic quantum critical point.

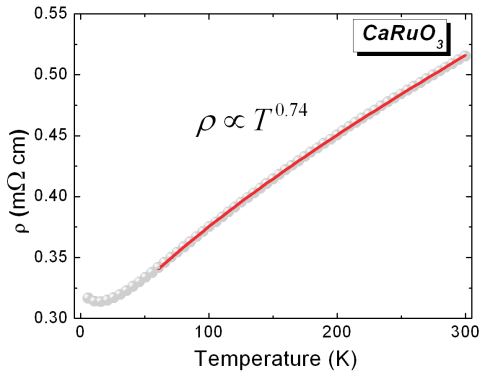


FIG. 2: Resistivity versus temperature of a $CaRuO_3$ film with thickness $\sim$ 100Å. The line shows the result of a power-law fit to the high-temperature range.

The resistivity of the $CaMnO_3$ film exhibits insulating, activated behavior (Fig. 3). A least-squares fit to the Arrhenius form $\rho(T) \propto \exp(E_a/k_BT)$ revealed two distinctive temperature regimes. For 300 K $\geq T \geq$ 175 K the data are described by $E_a = 31$ meV, while for 110 K $\geq T \geq$ 70 K, the fit yields $E_a = 48$ meV. Because the optical gap of $CaMnO_3$ is $\sim 1.5$ eV,[12] the transport is consistent with thermal excitation of carriers from a shallow impurity level below the conduction band, most likely due to oxygen defects.[13,14] Interestingly, the linear extrapolations of the fitted curves cross right at the Néel temperature $T_N = 125$ K. The difference in the

activation energies of 17 meV is therefore associated with the formation of magnetic polarons.[18] We note that this energy is in agreement with the activation energy for spin diffusion extracted from a recent nuclear magnetic resonance study of bulk $CaMnO_{3-x}$.[15] The wide intermediate range of temperatures between 175 and 110 K, where $\rho(T)$ deviates from the activated form, can therefore be associated with antiferromagnetic short-range order.

We now turn to the *dc* resistivity of the superlattices with $N = 4$ and $N = 10$ consecutive $CaRuO_3$ unit cells. The results displayed in Fig. 4 are qualitatively different from those of the constituents shown in Figs. 2 and 3. In particular, the resistivity of both samples exhibits a logarithmic temperature dependence $\rho \propto \ln(1/T)$ upon cooling below $T \sim 90$ K, a temperature close to the Néel temperature of the superlattices.[17] Whereas both reference films exhibit negligible magnetoresistance, the low-temperature resistivity of the superlattices strongly decreases in an external magnetic field, $H$, independent of whether it is applied parallel or perpendicular to the superlattice plane (Fig. 4). The corresponding magnetoresistance, defined as $[\rho(H) - \rho(0)]/\rho(0)$, amounts to 12.5 and 25 % for $N = 4$ and $N = 10$ samples, respectively, for $H = 8$ T (Fig. 5). This is qualitatively similar to, but larger than the MR determined by Takahashi *et al.*[6]

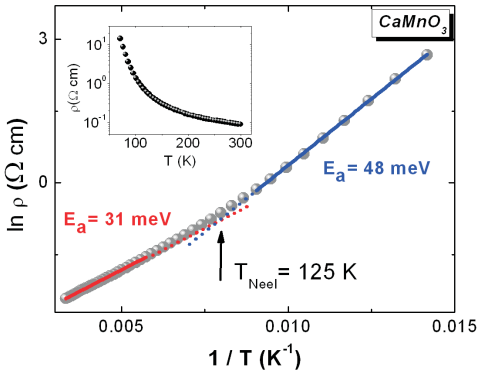


FIG. 3: Arrhenius plot of the temperature dependent resistivity of a $\sim$ 100Å thin film of $CaMnO_3$. The lines show the results of fits to exponentials with activation energies listed in the legend. The inset shows the data in log $\rho$-versus-$T$ plot.

In principle, a logarithmic term in the resistivity and negative MR can arise from weak localization.[20] The isotropic nature of the MR we observe in the $CaMnO_3$-$CaRuO_3$ superlattices, however, speaks against this interpretation and indicates a mechanism based on spin-dependent scattering. This is also supported by the observation that the onset of the logarithmic temperature dependence of the resistivity coincides approximately with the onset of magnetic order. Further, the weak hysteresis and absence of saturation of the MR is consistent with the magnetic field dependence of the net Mn magnetic moment in the magnetically ordered state.[17] Logarithmic terms in the temperature dependent resistivity have been reported for a wide variety of bulk materials within or close to magnetically ordered phases, including some heavy-fermion systems,[26] cuprate superconductors above their critical magnetic fields,[27–29] magnetic semiconductors such as $Fe_{1-x}Co_xS_2$,[30] and $CaRu_{1-x}Mn_xO_3$ solid solutions,[21–24] but the interpretation of these effects is still under debate. In the latter systems, Kondo scattering due to antiferromagnetic interactions between conduction electrons and localized Mn spins has been invoked to explain this behavior.[21] While the antiferromagnetic coupling was confirmed by a recent spectroscopic study,[25] quenched disorder due to chemical substitution, possibly associated with phase separation into domains with ferromagnetic and antiferromagnetic order, greatly complicate a quantitative analysis.[22–24]

Compared to the $CaRu_{1-x}Mn_xO_3$ solid solution, the trans-

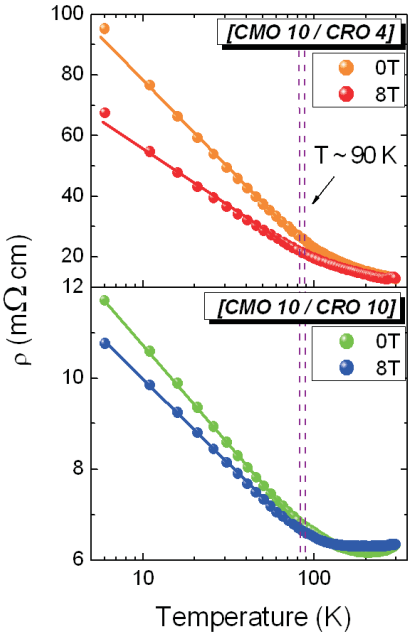


FIG. 4: Resistivity versus temperature for $CaRuO_3$-$CaMnO_3$ superlattices with $N = 4$ (upper panel) and $N = 10$ (lower panel) consecutive $CaRuO_3$ unit cells for $H = 0$ and 8 T (orange and red / green and blue circles, respectively). Note the logarithmic temperature scale. The straight solid lines (guide to the eyes) indicate a leading logarithmic term in the temperature dependence of resistivity below $T \sim 90$ K.

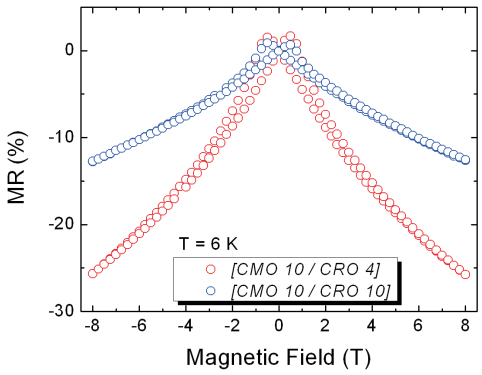


FIG. 5: *dc*-Magnetoresistance defined as $[\rho(H) - \rho(0)]/\rho(0)$ versus magnetic field $H$ of both superlattices at temperature $T = 6$ K.

port geometry in $CaMnO_3$-$CaRuO_3$ superlattices is better defined, and quenched disorder is greatly reduced. Nonetheless, one generally expects a nonvanishing influence of chemical, structural, and magnetic defects on the transport properties. In particular, in view of the negative MR observed in $CaRu_{1-x}Mn_xO_3$ (Ref. 23) one cannot rule out *a priori* that the MR observed in the superlattices is influenced by Mn-Ru intermixing at the interfaces. In order to assess the contribution of defects to the magnetoresistance, we have carried out optical conductivity measurements, which are much less affected by a small density of isolated defects.

### B. Far-infrared spectroscopy

Figure 6 shows near normal-incidence reflectivity spectra of both superlattice samples, along with those of a bare $LaAlO_3$ substrate and a $CaRuO_3$ single film on the substrate for comparison. Since the total thicknesses of the films are well below the far-IR wavelengths, the spectra are dominated by the contribution of the substrate, with the metallic response of $CaRuO_3$ superimposed on the $LaAlO_3$ phonon features. As a basis for a quantitative model of the reflectivity of the superlattices, we have acquired a reference spectrum of $LaAlO_3$ under the same experimental conditions. The reflectivity spectra of $LaAlO_3$ exhibit three main transverse optical (TO) phonon modes at 183 $cm^{-1}$, 427 $cm^{-1}$, and 648 $cm^{-1}$ and two longitudinal optical (LO) phonon modes at 277 $cm^{-1}$ and 596 $cm^{-1}$, in agreement with previous reports.[17,31] The high-frequency $LaAlO_3$-LO mode is located at 743 $cm^{-1}$, out of the investigated spectral range.

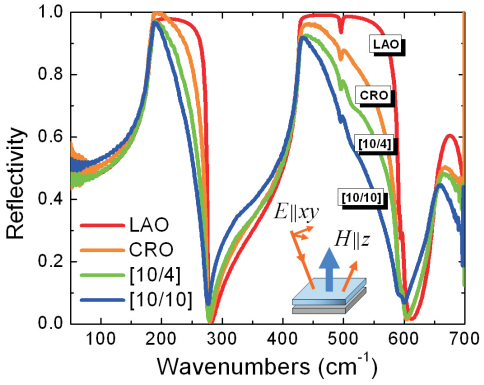


FIG. 6: Room temperature reflectivity spectra of a (001) $LaAlO_3$ substrate (marked as LAO), a $CaRuO_3$ film (marked as CRO), and the $N = 4$ and $N = 10$ superlattices. The inset shows the experimental geometry.

Magnetic field dependent reflectivity measurements were carried out for several temperatures in the range $3 \leq T \leq 300$ K, and magnetic fields $0 \leq H \leq 8$ T. When the temperature is reduced below $T \sim 200$ K, we observe clearly discernible magnetic field-induced changes in the reflectivity over a wide frequency range, for magnetic fields directed both parallel and perpendicular to the superlattice plane. Since the results for both field directions are identical within the experimental error, as in the corresponding $dc$-MR measurements, we present only data taken in the latter (Kerr) geometry, displayed as the ratio $R(\omega, H)/R(\omega, 0)$ at $T = 3$ K in Fig. 7. The specific shape of the spectral features in this plot is caused by singularities in the reflectivity of the $LaAlO_3$ substrate at frequencies where the real part of the dielectric function crosses zero. Thus, the moderate magnetic field dependence of the optical conductivity of itinerant charge carriers in the superlattice results in sharp magnetoreflection peaks near the $LaAlO_3$-LO mode eigenfrequencies.

In our analysis, we treated the superlattices within the effective-medium approach, *i.e.* as a single composite layer with thickness equal to that of the respective sample.[17,32,33] This approximation is justified, because the sample thicknesses are well below the wavelengths in the FIR range. In order to quantitatively determine the FIR magnetoresistance, we fitted the magnetoreflection spectra in Fig. 7 to the model spectra of a single Drude-metal layer on a semi-infinite $LaAlO_3$ substrate following a regression procedure provided by software packages for the characterization of multilayers[34]. The initial zero-magnetic field model parameters were selected following a prior ellipsometry study,[17] where the complex dielectric function of the superlattices was described by a broad Drude response, $\varepsilon(\omega) = \varepsilon_\infty - \omega_{pl}^2/(\omega^2 + i\omega\gamma)$, with a ratio of scattering rate and plasma frequency of $\gamma/\omega_{pl}$ = 0.2 - 0.3, $\varepsilon_\infty$ is the high-frequency contribution to the dielectric function. In the far-IR range for $\omega \ll \gamma \approx 3000$ $cm^{-1}$, $\varepsilon(\omega)$ is almost frequency independent. The measurements thus accurately determine the ratio $\omega_{pl}^2/\gamma$, which represents the zero-frequency limit of the infrared conductivity, $\sigma_{\omega\to 0} = 1/\rho_{\omega\to 0} = 1/4\pi \times \omega_{pl}^2/\gamma$. Figure 7 shows that a fit with this ratio as the only free parameter yields a good description of the magnetic field dependent reflectivity of both superlattices over the entire FIR frequency range. We have thus demonstrated that the combination of reflectivity and ellipsometry data allows an accurate extrapolation of the optical data to zero frequency. The temperature and field dependent resistivity $\rho_{\omega\to 0} \propto \gamma/\omega_{pl}^2$ determined in this way are presented in Figs. 8 and 9, respectively.

We now compare the results of the $\omega \to 0$ extrapolation of the optical data, $\rho_{\omega\to 0}$ and $MR_{\omega\to 0}$, shown in Figs. 8 and 9 with their counterparts resulting from $dc$ transport measurements, $\rho$ and MR, in Figs. 4 and 5. At high temperatures, the temperature evolution of $\rho$ and $\rho_{\omega\to 0}$ is similar, but $\rho$ is about a factor of 4 larger than $\rho_{\omega\to 0}$. Such differences between both quantities are commonly observed as a result of a small density of isolated, extended defects such as dislocations or microcracks that disrupt the current flow over macroscopic distances, but do not affect the local response to alternating electric fields. Indeed, x-ray reflectivity data on our samples[17] have revealed an effective structural interface roughness of about 5 Å, which is common for oxide superlattices[35,36] and likely originates in a small density of stacking faults or dislocations nucleated by atomic steps or twin boundaries on the substrate surface. Prior studies of bulk transition metal oxides using a methodology similar to ours[37] have shown that such microstructural defects yield a temperature-independent contribution to the $dc$ resistivity, in agreement with the super-

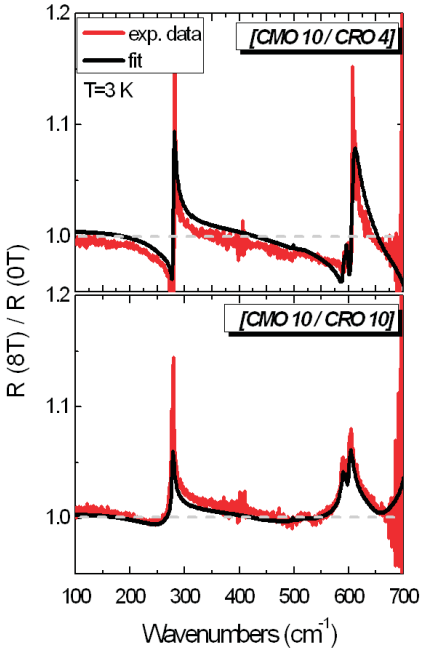


FIG. 7: Ratio of reflectivity spectra taken for magnetic fields $H = 8$ and 0 T for $N = 4$ (upper panel) and $N = 10$ (lower panel) superlattices. The solid lines are the results of model calculations described in the text.

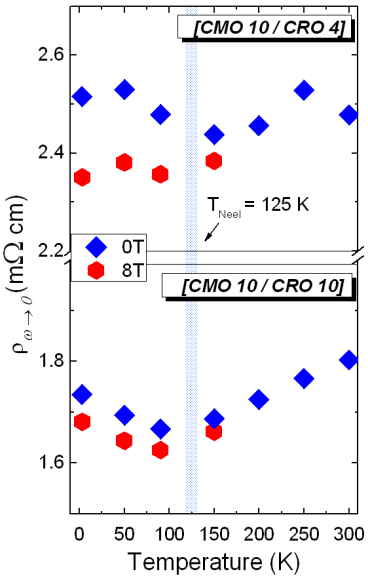


FIG. 8: Temperature dependent resistivity extracted from the extrapolation of the optical response in magnetic fields $H = 0$ and 8 T for $N = 4$ (upper panel) and $N = 10$ superlattices (lower panel). The shaded line marks the Néel temperature.

lattice data above $T_N$.

Upon cooling below $T_N$, however, the $dc$ and FIR responses exhibit profoundly different behavior. In particular, $\rho$ exhibits a pronounced upturn and diverges logarithmically as $T \to 0$, which can be attributed to a spin-dependent scattering mechanism, as discussed in Section II. $\rho_{\omega\to 0}$, on the other

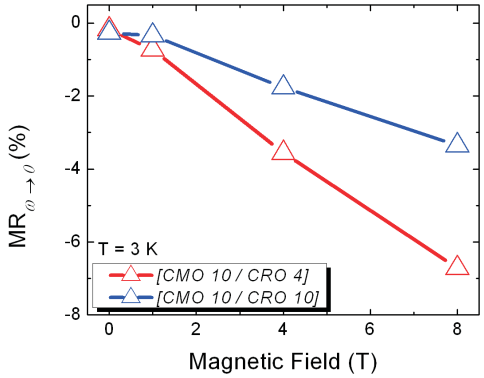


FIG. 9: Magnetoresistance defined as $[\rho_{\omega\to 0}(H) - \rho_{\omega\to 0}(0)]/\rho_{\omega\to 0}(0)$ extracted from the extrapolation of the FIR optical response to zero frequency, for both superlattices at temperature $T = 3$ K.

hand, exhibits at most a subtle upturn upon cooling below $T_N$. At low temperatures, both MR and $\mathrm{MR}_{\omega\to 0}$ are qualitatively similar. In particular, they do not show saturation at high fields and exhibit the same ratio of $\sim 2:1$ between $N = 4$ and $N = 10$ superlattices, confirming that spin-dependent scattering is the dominant source of resistivity at low temperatures. The absolute magnitudes of MR and $\mathrm{MR}_{\omega\to 0}$ are, however, very different. This discrepancy indicates that the magnetic scattering centers responsible for the logarithmic term in the temperature dependence are sparse and spatially isolated, so that they affect the $dc$ current flow much more than the optical conductivity. This rules out short-range interface roughness generated, for instance, by uniform Ru-Mn intermixing as the origin of the MR. Comparison with soft x-ray reflectometry data[17] suggests a different mechanism of this effect. These experiments have provided evidence of spin polarization due to magnetic polarons in the $CaMnO_3$ layers, analogous to those previously observed in bulk $CaMnO_3$.[13,14,18] Scattering of charge carriers in the atomically thin $CaRuO_3$ layers from polaronic defects trapped at structural faults in the superlattice may then act as spin-dependent transport bottlenecks, thus generating a large $dc$ magnetoresistance effect.

## IV. CONCLUSIONS

A detailed comparison of the $dc$- and FIR-magnetoresistance in $CaMnO_3$-$CaRuO_3$ superlattices has revealed large differences below the Néel temperature of $CaMnO_3$, which are attributable to scattering of charge carriers in $CaRuO_3$ from sparse, isolated magnetic defects near the interfaces. These scattering processes generate a contribution to the $dc$-resistivity that diverges logarithmically as $T \to 0$. The same experimental approach may also be useful in exploring the origin of similar logarithmic terms in the low-temperature resistivities of a variety of bulk systems.[21–24,26–30] In contrast to bulk solid solutions, the $CaMnO_3$-$CaRuO_3$ superlattices have the advantage that the contact between the itinerant charge carriers and the magnetic

scattering centers is limited to well-defined interfaces. Tailoring of spin textures at these interfaces may therefore open up new perspectives for functional oxide devices.

### Acknowledgments

Work in Stuttgart was partially supported by the German Science Foundation under collaborative Grant No. SFB/TRR80. Work at Argonne, including the Advanced Photon Source, and the Center for Nanoscale Materials is supported by the U.S. Department of Energy, Office of Science, under Contract No. DE-AC02-06CH11357. J.C. was supported by DOD-ARO under Grant No. W911NF-08-1-0186 and NSF under Contract No. DMR-0747808. H.N.L. was sponsored by the Materials Sciences and Engineering Division, Office of Basic Energy Sciences, U.S. Department of Energy.

[1] C. Adamo, X. Ke, P. Schiffer, A. Soukiassian, M. Warusawithana, L. Maritato, and D. G. Schlom, Appl. Phys. Lett. **92**, 112508 (2008).

[2] A. Bhattacharya, S. J. May, S. G. E. te Velthuis, M. Warusawithana, X. Zhai, Bin Jiang, J.-M. Zuo, M. R. Fitzsimmons, S. D. Bader, and J. N. Eckstein, Phys. Rev. Lett. **100**, 257203 (2008).

[3] H. Yamada, P.H. Xiang, and A. Sawa, Phys. Rev. B **81**, 014410 (2010).

[4] A. Brinkman, M. Huijben, M. Van Zalk, J. Huijben, U. Zeitler, J. C. Maan, W. G. Van Der Wiel, G. Rijnders, D. H. A. Blank and H. Hilgenkamp, Nature Mater. **6**, 493 (2007).

[5] A. D. Caviglia, M. Gabay, S. Gariglio, N. Reyren, C. Cancellieri, and J.-M. Triscone, Phys. Rev. Lett. **104**, 126803 (2010).

[6] K. S. Takahashi, M. Kawasaki, and Y. Tokura, Appl. Phys. Lett. **79**, 1324 (2001).

[7] H. Yamada, H. Sato, H. Akoh, N. Kida, T. Arima, M. Kawasaki, and Y. Tokura, Appl. Phys. Lett. **92**, 062508 (2008).

[8] G. Cao, O. Korneta, S. Chikara, L. E. DeLong, and P. Schlottmann, Solid State Comm. **148**, 305 (2008).

[9] L. Klein, L. Antognazza, T. H. Geballe, M. R. Beasley, and A. Kapitulnik, Phys. Rev. B **60**, 1448 (1999).

[10] L. Capogna, A. P. Mackenzie, R. S. Perry, S. A. Grigera, L. M. Galvin, P. Raychaudhuri, A. J. Schofield, C. S. Alexander, G. Cao, S. R. Julian, and Y. Maeno, Phys. Rev. Lett. **88**, 076602 (2002).

[11] Y. S. Lee, Jaejun Yu, J. S. Lee, T. W. Noh, T.-H. Gimm, Han-Yong Choi, and C. B. Eom, Phys. Rev. B **66**, 041104 (2002).

[12] N. N. Loshkareva, L. V. Nomerovannaya, E. V. Mostovshchikova, A. A. Makhnev, Yu. P. Sukhorukov, N. I. Solin, T. I. Arbuzova, S. V. Naumov, N. V. Kostromitina, A.M. Balbashov, and L.N. Rybina, Phys. Rev. B **70**, 224406 (2004).

[13] J. J. Neumeier and J.L. Cohn, Phys. Rev. B **61**, 14319 (2000).

[14] C. Chiorescu, J. L. Cohn, and J. J. Neumeier, Phys. Rev. B **76**, 020404 (2007).

[15] A. Trokiner, S. Verkhovskii, A. Yakubovskii, A. Gerashenko, P. Monod, K. Kumagai, K. Mikhalev, A. Buzlukov, Z. Litvinova, O. Gorbenko, A. Kaul, and M. Kartavtzeva, Phys. Rev. B **79**, 214414 (2009).

[16] B. R. K. Nanda, S. Satpathy, and M. S. Springborg, Phys. Rev. Lett. **98**, 216804 (2007).

[17] J. W. Freeland, J. Chakhalian, A. V. Boris, J.-M. Tonnerre, J. J. Kavich, P. Yordanov, S. Grenier, P. Zschack, E. Karapetrova, P. Popovich, H. N. Lee, and B. Keimer, Phys. Rev. B **81**, 094414 (2010).

[18] H. Meskine, T. Saha-Dasgupta, and S. Satpathy, Phys. Rev. Lett. **92**, 056401 (2004); H. Meskine and S. Satpathy, J. Phys. Condens. Matter **17**, 1889 (2005).

[19] E.B. McDaniel and J.W.P. Hsu, J. Appl. Phys. **80**, 1085 (1996).

[20] For a review, see P. A. Lee and T. V. Ramakrishnan, Rev. Mod. Phys. **57**, 287 (1985).

[21] T. Sugiyama and N. Tsuda, J. Phys. Soc. Jpn. **68**, 1306 (1999).

[22] A. Maignan, C. Martin, M. Hervieu, and B. Raveau, Solid State Comm. **117**, 377 (2001).

[23] L. Pi, S. Hébert, C. Martin, A. Maignan, and B. Raveau, Phys. Rev. B **67**, 024430 (2003).

[24] V. Markovich, M. Auslender, I. Fita, R. Puzniak, C. Martin, A. Wisniewski, A. Maignan, B. Raveau, and G. Gorodetsky, Phys. Rev. B **73**, 014416 (2006).

[25] K. Terai, K. Yoshii, Y. Takeda, S. I. Fujimori, Y. Saitoh, K. Ohwada, T. Inami, T. Okane, M. Arita, K. Shimada, H. Namatame, M. Taniguchi, K. Kobayashi, M. Kobayashi, and A. Fujimori, Phys. Rev. B **77**, 115128 (2008).

[26] For a review, see H. von Löhneysen, A. Rosch, M. Vojta, and P. Wölfle, Rev. Mod. Phys. **79**, 1015 (2007).

[27] Y. Ando, G. S. Boebinger, A. Passner, T. Kimura and K. Kishio, Phys. Rev. Lett. **75**, 4662 (1995).

[28] S. Ono, Y. Ando, T. Murayama, F. F. Balakirev, J. B. Betts, and G. S. Boebinger, Phys. Rev. Lett. **85**, 638 (2000).

[29] T. Sekitani, M. Naito, and N. Miura, Phys. Rev. B **67**, 174503 (2003).

[30] S. Guo, D. P. Young, R. T. Macaluso, D. A. Browne, N. L. Henderson, J. Y. Chan, L. L. Henry, and J. F. DiTusa, Phys. Rev. Lett. **100**, 017209 (2008).

[31] A.V. Boris, N.N. Kovaleva, A.V. Bazhenov, A.V. Samoilov, N.C. Yeh, and R.P. Vasquez, J. Appl. Phys. **81**, 5756 (1997).

[32] A. Dubroka, G. Cristiani, H.-U. Habermeier, and J. Humlicek, Thin Solid Films **455-456**, 172 (2004).

[33] S. S. A. Seo, W. S. Choi, H. N. Lee, L. Yu, K.W. Kim, C. Bernhard, and T.W. Noh, Phys. Rev. Lett. **99**, 266801 (2007).

[34] A. V. Tikhonravov and M. K. Trubetskov, OPTILAYER thin film software, http://www.optilayer.com; A. Kuzmenko, RefFIT software package, University of Geneva, http://optics.unige.ch/alexey/reffit.html.

[35] J. Stahn, J. Chakhalian, Ch. Niedermayer, J. Hoppler, T. Gutberlet, J. Voigt, F. Treubel, H-U. Habermeier, G. Cristiani, B. Keimer, and C. Bernhard, Phys. Rev. B **71**, 140509(R) (2005).

[36] E. Benckiser, M. W. Haverkort, S. Brück, E. Goering, S. Macke, A. Franó, X. Yang, O. K. Andersen, G. Cristiani, H.-U. Habermeier, A. V. Boris, I. Zegkinoglou, P. Wochner, H.-J. Kim, V. Hinkov, and B. Keimer, Nature Mater. **10**, 189 (2011).

[37] A. Lebon, P. Adler, C. Bernhard, A.V. Boris, A.V. Pimenov, A. Maljuk, C.T. Lin, C. Ulrich, and B. Keimer, Phys. Rev. Lett. **92**, 037202 (2004).